

Efficient Domain Coverage for Vehicles with Second Order Dynamics via Multi-Agent Reinforcement Learning

Xinyu Zhao, Razvan C. Fetecau, Mo Chen

Abstract—Collaborative autonomous multi-agent systems covering a specified area have many potential applications, such as UAV search and rescue, forest fire fighting, and real-time high-resolution monitoring. Traditional approaches for such coverage problems involve designing a model-based control policy based on sensor data. However, designing model-based controllers is challenging, and the state-of-the-art classical control policy still exhibits a large degree of suboptimality. In this paper, we present a reinforcement learning (RL) approach for the multi-agent coverage problem involving agents with second-order dynamics. Our approach is based on the Multi-Agent Proximal Policy Optimization Algorithm (MAPPO). To improve the stability of the learning-based policy and efficiency of exploration, we utilize an imitation loss based on the state-of-the-art classical control policy. Our trained policy significantly outperforms the state-of-the-art. Our proposed network architecture includes incorporation of self attention, which allows a single-shot domain transfer of the trained policy to a large variety of domain shapes and number of agents. We demonstrate our proposed method in a variety of simulated experiments.

Index Terms—Multi-Robot Systems, Reinforcement Learning, Domain Coverage, Self-Attention, Imitation Learning

I. INTRODUCTION

Multi-agent cooperative area coverage is an active research field, with the objective being to deploy a set of agents over a domain of interest to achieve optimal sensing. Applications include monitoring [1], [2], target detection [3], [4], and search and rescue [5], [6]. In the past decades, researchers have proposed various methods to solve coverage problems. One common approach is to perform coverage control via an optimization problem that involves Voronoi tessellations [7], [8]. Other popular approaches include potential field methods [9]–[11], and scalar field mapping [12]–[14]. Although these methods have been proven to be effective, they are mostly concerned with the steady state agent configuration and do not directly address time efficiency in achieving coverage.

In this paper, we propose using deep reinforcement learning (RL) as a means to remedy some challenges in classical model-based controllers. In general, deep RL could leverage the advantages of neural networks (NNs) and adaptive learning capabilities to obtain a policy that optimizes the performance metric over the trajectory. NNs have the ability to approximate a broad class of functions, and through RL, a control policy parameterized by a NN can be directly learned through real-time interactive feedback from the environment, and hence avoiding the challenge of choosing an accurate model.

This work has been submitted to the IEEE for possible publication. Copyright may be transferred without notice, after which this version may no longer be accessible.

X. Zhao and R. C. Fetecau are with the Department of Mathematics, Simon Fraser University, Burnaby, BC, Canada (SFU) {xza261@, van@math.}sfu.ca). M. Chen is with the School of Computing Science, SFU, mochen@cs.sfu.ca.

This work received support from Huawei Technologies Co., Ltd.

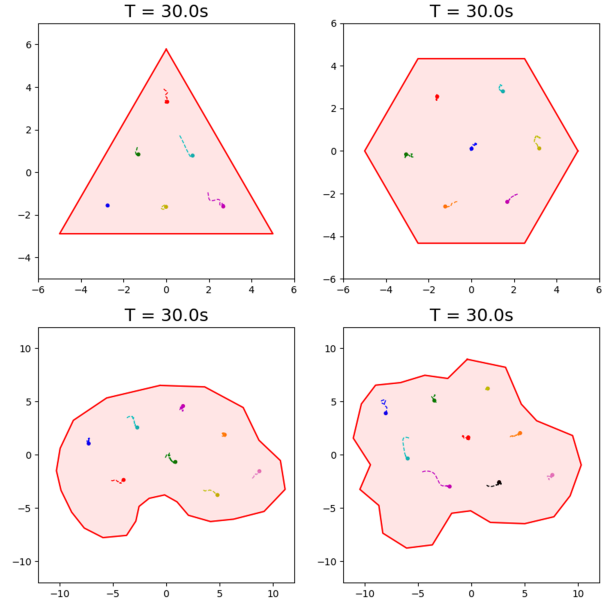


Fig. 1: The final coverage configuration of our policy for 6 agents in a triangle, 7 agents in a hexagon, and 8 and 9 agents in non-convex domains. The tails in all plots represent the agents’ trajectories in the last 15s of simulation. The simulation duration is 30s and our policy achieves good coverage within 20s. The small perturbations over the last 15s indicate reliable persistent coverage performance.

Many previous works on applying multi-agent RL to coverage problems applied value-based methods, such as DQN and SARSA, to systems with discrete action space, using either centralized and decentralized learning [15]–[18]. To our best knowledge, only two papers have applied MARL to an environment with continuous action space for the coverage task. In [19], the authors proposed applying an actor-critic method to multi-agent continuous coverage control. The authors in [20] used MADDPG [21] to learn a continuous coverage controller for an ocean monitoring task.

In this work, we propose a method that combines classical coverage control with self-attention-based RL. We aim to learn a policy that 1) allows the agents to achieve the final coverage configuration in a time efficient manner, and 2) has the ability to handle a varying number of agents and can adapt to a variety of domains. For an illustration, Fig. 1 shows final coverage configurations achieved with our policy, with 6 to 9 agents, for both symmetric and non-symmetric domains.

Our contributions are as follows:

- We propose an MARL approach for the domain coverage problem, using a controller with double integrator dy-

namics. We use a reward function based on the artificial potentials of the controller.

- Compared to the controller, the MARL approach has better time efficiency to reach coverage.
- We combine online and offline learning in a simple way to improve training stability.
- We use a self-attention-based critic network to improve policy generalization.

The rest of the paper is organized as follows. Section II states the problem formulation for domain coverage. Section III provides background information. Section IV gives details on our approach for solving the efficient coverage control across various domains and different numbers of agents. Section V illustrates our approach with numerical simulations.

II. PROBLEM FORMULATION

We consider a set of n homogeneous agents indexed by $I = \{1, \dots, n\}$, with dynamics given by

$$\begin{cases} \dot{p}^i = v^i, & \|v^i\| \leq v_{max}, \\ \dot{v}^i = a^i, & \|a^i\| \leq a_{max}, \end{cases} \quad (1)$$

where $p^i = (p_x^i, p_y^i)$, $v^i = (v_x^i, v_y^i)$ and $a^i = (a_x^i, a_y^i)$ are the position, velocity and the control input of the i th agent, respectively. Also, v_{max} and a_{max} are bounds on velocities and control inputs, and $\|\cdot\|$ is the Euclidean distance.

The problem definition of multi-agent area coverage can vary under different scenarios and assumptions. In this paper, we are interested in deploying the set of agents into a target domain to achieve uniform area coverage. Specifically, we adopt the concept of coverage presented in [11], [22].

Definition II.1. We say that the group of agents I is an l -*subcover* configuration for a compact domain $\Omega \subset \mathbb{R}^2$ if

1. $B_{\frac{l}{2}}(i) \subset \Omega$ for all $i \in I$,
2. $\|p^i - p^j\| \geq l$ for all pairs $i, j \in I$, $i \neq j$.

where $B_{\frac{l}{2}}(i)$ denotes the ball of radius $\frac{l}{2}$ centered at p^i .

The main interest in [11] is in l_d -*subcover* configurations, where $l_d = \sqrt{\frac{\text{Area}(\Omega)}{n}}$, based on the assumption that each agent covers the same amount of square area (uniform coverage). Aside from reaching an l_d -*subcover* configuration, we are also interested in the time efficiency of achieving domain coverage. Based on Def. II.1 and the time efficiency concerns, the primary interest of this work is defined as follows.

Multi-Agent Efficient Domain Coverage Control: We aim to find a control policy that drives a set of n agents from any initial positions to an l_d -*subcover* of some compact domain Ω as quickly as possible.

III. BACKGROUND

In this section, we review some important background information for this work. We consider multi-agent domain coverage control as a fully cooperative task with homogeneous agents, which can be formulated as a decentralized partially observable Markov decision process (Dec-POMDP) [23] of n agents consisting of a tuple of $\langle S, A, O, P, R, n, \gamma \rangle$. Here, S is the joint state space of all agents, A is the joint action space of

all agents, O is the joint observation space, $P = \mathbb{P}(s_{t+1}|s_t, a)$ is the transition probability function from current joint state s_t to the next state s_{t+1} given the joint action $a = (a^1, \dots, a^n)$, $R(s_t, a, s_{t+1}): S \times A \times S \rightarrow \mathbb{R}$ is the global reward function based on a joint state and action pair, n is the number of agents, and $\gamma \in [0, 1)$ is a constant discount factor.

The joint state s is only partially observable to each agent, who draws the local observation o^i according to its own observation function $\eta^i: S \rightarrow O$. At time t , each agent samples an action a_t^i from a stochastic policy $\pi^i(a_t^i|o_t^i)$ given o_t^i . By executing the joint action $a_t = (a_t^1, \dots, a_t^n)$, the joint state evolves from s_t to s_{t+1} according to the transition probability function P , and an immediate reward $R_t = R(s_t, a_t, s_{t+1})$ is given by the environment. The return G_t is defined as the discounted cumulative future reward starting from state s_t , given by $G_t = \sum_{k=0}^T \gamma^k R_{t+k}$.

The objective for all agents is to find a joint policy $\pi = (\pi^1, \dots, \pi^n)$ that maximizes the corresponding state value function $V^\pi(s) = \mathbb{E}_\pi[G_t|s_t = s]$ for any given state s .

A. Multi-Agent Proximal Policy Optimization

Our approach is built upon multi-agent proximal policy optimization (MAPPO) [24], which is a popular actor-critic algorithm for the MARL problem. The main feature of MAPPO is to extend the PPO algorithm [25] under the centralized training and decentralized execution (CTDE) framework [21]. In particular, the CTDE extension for any actor-critic architecture allows the critic network to access the environment's global state, while the policy network for every agent still chooses the action based on the agent's local observation only.

Consider an n -agent environment described by Dec-POMDP, with a set of policies $\pi_\theta = (\pi_{\theta^1}, \dots, \pi_{\theta^n})$ parametrized by $\theta = (\theta^1, \dots, \theta^n)$, and a centralized value function V_ϕ parametrized by ϕ . The MAPPO algorithm samples trajectories from an old joint policy $\pi_{\theta_{old}}$, and updates the policy parameter for each agent by maximizing the following surrogate objective

$$J(\theta^i) = \mathbb{E}_{s \sim \rho_{\pi_{\theta_{old}}}, a^i \sim \pi_{\theta_{old}}^i} \left[\min(r_t(\theta^i) A_{\pi_{\theta_{old}}}(s_t, a_t), \text{clip}(r_t(\theta^i), 1 + \epsilon, 1 - \epsilon) A_{\pi_{\theta_{old}}}(s_t, a_t)) \right], \quad (2)$$

where $\rho_{\pi_{\theta_{old}}}$ is the state visitation frequency induced by old policy $\pi_{\theta_{old}}$, $r_t(\theta^i)$ is the probability ratio calculated as

$$r_t(\theta^i) = \frac{\pi_{\theta^i}(a_t^i|\eta^i(s_t))}{\pi_{\theta_{old}^i}(a_t^i|\eta^i(s_t))}, \quad (3)$$

$A_{\pi_{\theta_{old}}}(s_t, a_t)$ is the advantage value at time t , and $\epsilon \in [0, 1)$ is a hyperparameter controlling the clip rate. Moreover, the above objective without the clip term is also referred to as the objective of conservative policy iteration (CPI) [26].

The advantage function $A_{\pi_{old}}(s_t, a_t)$ can be estimated in several ways as in [27] based on the centralized value function V_ϕ , which is found by minimizing the standard mean squared error loss (MSE) between $V_\phi(s_t)$ and a value target \hat{V}_t such as a Monte-Carlo estimation or temporal-difference target. For more details about the PPO and MAPPO objective, we refer the reader to [24], [25].

B. Behaviour Cloning

Instead of learning through interacting with the environment, behaviour cloning (BC) tries to copy an expert's policy using supervised learning. For a stochastic policy π_θ , BC minimizes the error between the expert's action and the maximum likelihood action over the current policy. Such a minimization problem could be done by minimizing several different objective functions. Our approach uses a simple version of BC, where the objective is given by

$$L^{BC}(\pi) = \frac{1}{\mathcal{T}} \sum_{t=0}^{\mathcal{T}} \|\hat{a}_t^i - \mu_{\pi_\theta}(o_t^i)\|^2, \quad (4)$$

where \hat{a}_t^i is the expert's action under the observation o_t^i , and $\mu_{\pi_\theta}(o_t^i)$ is the mean of stochastic policy π_θ .

IV. APPROACH

In this section, we explain the details of our approach for applying MARL to solve the multi-agent efficient domain coverage control problem defined in Sec. II. Two major challenges need to be addressed: The learned policies need to 1) produce a time efficient trajectory while completing the coverage task, and 2) be generalized for multiple scenarios involving different domains and number of agents.

To address the two challenges above, we build our method based on the MAPPO algorithm with newly designed policy and value network architectures. In order to guide the agent to learn a suitable control policy that solves the multi-agent coverage problem efficiently, a proper reward function needs to be designed. We accomplish this by choosing a suitable potential function from the classical coverage control. With an adequately shaped reward, agents learning to maximize the return also improve time efficiency.

The policy generalization in this work specifically refers to using a single policy for environments with different numbers of agents in various domains. We address this challenge by training the policy concurrently across multiple environments with a variable number of agents. In order to enable such a learning process, our approach utilizes the parameter sharing on both policy and critic networks, leverages the long short term memory (LSTM) and the Self-Attention structures, and facilitates the training with direct value decomposition.

An overview of our approach is illustrated in Fig. 2. The "Actor" and "Critic" parts of the figure will be explained in detail in Sections IV-C and IV-D, respectively.

A. Agent Observation and Environment State

We first specify the assumptions on the environment state and agent observation in this work. We assume that every agent knows its own position p^i and velocity v^i . We further assume that every agent can measure its position relative to the domain boundary $\partial\Omega$, given by the vector

$$d^i := p^i - P_{\partial\Omega}(p^i), \quad (5)$$

where $P_{\partial\Omega}$ denotes the projection operator to $\partial\Omega$. With these assumptions, we define the agent's internal state s^i to be

$$s^i = (p^i, v^i, \hat{d}^i, \|d^i\|, \mathbb{I}(p^i)), \quad (6)$$

where $\hat{d}^i = d^i / \|d^i\|$ and $\mathbb{I}(p^i)$ is given by

$$\mathbb{I}(p^i) = \begin{cases} 1, & \text{if } p^i \notin \Omega, \\ -1, & \text{if } p^i \in \Omega. \end{cases} \quad (7)$$

We further construct the environment full state s by stacking all s^i as

$$s = \begin{bmatrix} s^1 \\ \vdots \\ s^n \end{bmatrix} = \begin{bmatrix} p^1 & v^1 & \hat{d}^1 & \|d^1\| & \mathbb{I}(p^1) \\ \vdots & \vdots & \vdots & \vdots & \vdots \\ p^n & v^n & \hat{d}^n & \|d^n\| & \mathbb{I}(p^n) \end{bmatrix}. \quad (8)$$

The expression of state as a matrix will be useful in Sec. IV-D.

Partial observability in this paper means that agents do not know all the information about the other agents. However, we assume that each agent knows its position relative to the other agents, represented by $p^{i,j} = p^i - p^j$ for $i \neq j$. Therefore, we consider the agent local observation $o^i = (s^i, \tilde{o}^i)$ to consist of two parts, where the first part is the agent's internal state s^i and the second part is the observation of other agents relative to itself, given by

$$\tilde{o}^i = (p^{i,1}, p^{i,2}, \dots, p^{i,i-1}, p^{i,i+1}, \dots, p^{i,n}).$$

In practice, such an observation can be obtained by ranging sensors such as LIDAR.

B. Reward Shaping

We now discuss reward shaping for the domain coverage problem stated in Sec. II. We design the reward function to address the coverage goal, as well as time efficiency. We base our reward function on the artificial potentials used in [11], [22] for the dynamics of (1). Specifically, the potential functions in [11], [22] for agent-domain and inter-agent interactions, are given respectively by

$$U_h(p^i) = \begin{cases} 0, & \text{for } \llbracket d^i \rrbracket \leq -\frac{l_d}{2}, \\ \frac{1}{2}(\llbracket d^i \rrbracket + \frac{l_d}{2})^2, & \text{for } \llbracket d^i \rrbracket > -\frac{l_d}{2}, \text{ and} \end{cases} \quad (9a)$$

$$U_I(p^{i,j}) = \begin{cases} \frac{1}{2}(\|p^{i,j}\| - l_d)^2, & \text{for } \|p^{i,j}\| < l_d, \\ 0, & \text{for } \|p^{i,j}\| \geq l_d. \end{cases} \quad (9b)$$

Here, $\llbracket d^i \rrbracket$ denotes the signed distance of p^i from $\partial\Omega$, i.e.,

$$\llbracket d^i \rrbracket = \mathbb{I}(p^i) \cdot \|p^i - P_{\partial\Omega}(p^i)\|. \quad (10)$$

Note that the expressions of U_h and U_I correspond directly to the two conditions in Def. II.1 (for $l = l_d$).

The total potential energy of the system is given by

$$\Phi = \sum_i^n \Phi^i, \quad (11)$$

where Φ^i is the individual potential obtained by summing up U_h and U_I as

$$\Phi^i = 2U_h(p^i) + \sum_{j \neq i}^n U_I(p^{i,j}). \quad (12)$$

The global minimum of Φ is zero and attained at l_d -subcover configurations and is a measure for coverage performance. In our method, we shape the reward by transforming

the potential energy slightly. We define the agent’s individual reward $R^i(s_t, a_t, s_{t+1})$ as

$$R^i(s_t, a_t, s_{t+1}) = \begin{cases} -M, & \text{if agent } i \text{ is outside } \Omega, \\ -\Phi_{t+1}^i, & \text{if agent } i \text{ is inside } \Omega. \end{cases} \quad (13)$$

where M is a positive constant, and Φ_{t+1}^i denotes the individual potential for agent indexed by i at time step $t + 1$. Here, a constant reward $-M$ is assigned to an agent that is outside the domain, as the potential could be arbitrarily large in such case. We set the constant M to be

$$M = \sup\{\Phi : \text{all agents are inside } \Omega\}.$$

We further define R as the global reward for the Dec-POMDP setup, which is calculated by taking the sum of all agents’ individual rewards, i.e.,

$$R(s_t, a_t, s_{t+1}) = \sum_{i=1}^n R^i(s_t, a_t, s_{t+1}). \quad (14)$$

Let $R_t^i = R^i(s_t, a_t, s_{t+1})$, and $R_t = R(s_t, a_t, s_{t+1})$. The formulation in (14) allows each agent to receive a different reward, while simultaneously knowing its contribution to the team. We remark that the additive reward formulation allows us to use the direct value decomposition, which facilitates the training process in our approach. Details on using the reward (14) will be presented in Sec. IV-D.

The reward design in (14) also naturally fits into the purpose of maximizing time efficiency. It is clear that the maximum of R is zero and can be attained at any l_d -subcover configuration. Hence, a trajectory that attains the coverage goal faster will gain higher returns. Since the objective of RL is to find a policy that maximizes the expected returns, the policy learned through the reward (14) is expected to improve time efficiency.

C. Actor Architecture for Variable Length Input

A typical policy network architecture in MARL uses a multiple-layer perceptron (MLP) for each agent. However, such architecture has difficulties generalizing the policy into the scenario of a variable number of agents. In this work, we utilize the parameter sharing (PS) technique [28], [29], where all homogeneous agents share a single policy network $\pi_{\theta^1} = \dots = \pi_{\theta^n}$. The PS technique naturally fits into the purpose of training a single policy to handle a variable number of agents, as the shared policy offers different actions for different agents based on observation from each agent.

Although a shared policy makes the policy suitable for a variable number of agents, the MLP cannot handle the variable length input of observation caused by the variable number of agents. Therefore, for the policy network, we use the LSTM architecture, a popular recurrent NN [30], which accepts a variable length input and produces a fixed-length output.

Besides being able to take as input vectors of varying length, another advantage of the LSTM for multi-agent coverage control is that it takes an *ordered* sequence as input. In our problem definition, the variable length part of the input is \tilde{o}^i , an agent’s relative observation, which can be naturally treated as a sequence ordered according to the relative importance of other agents. In our application of the LSTM architecture, for every time step t , the first entry of \tilde{o}_t^i will be fed first

and produce a hidden state inside the LSTM. When the next entry is fed in, the LSTM will combine both the current entry and the hidden vector from the last entry to produce the next hidden vector. Eventually, the entire input \tilde{o}^i is mapped to the final hidden vector, denoted as h_t^i , which represents an encoded vector that stores all the important information in \tilde{o}^i . Later entries have more direct influence in the LSTM output.

Therefore, we arrange the entries in \tilde{o}^i in descending order of the norm. Such an ordering puts the relative position of the farthest agent first, and of the nearest agent last, and captures the intuition that nearby agents should have a stronger effect on the current agent’s action. This ordering is also consistent with the agent interaction potential U_I , where two agents interact more strongly if they are closer to each other.

The LSTM output h_t^i is concatenated with the agents’ internal state s^i and fed into the standard MLP to output the policy distribution. The LSTM-based actor network is illustrated in the “Actor” part of Fig. 2.

D. Self-Attention Based Value Decomposition Network

With the CTDE framework, the shared critic network takes the global state s as input to estimate the true state value, where s is of variable length according to the number of agents. While one can attempt a similar procedure as in Sec. IV-C for the environment state and treat s as a sequence of the agents’ internal states s^i , the LSTM structure is not the most appropriate for the *centralized* critic network since there is no natural agent ordering. We propose instead a self-attention based value-decomposition structure, which is able to estimate the state value by equally assessing all agents’ internal states s^i . This structure is illustrated in the “Critic” part of Fig. 2.

The self-attention was originally introduced in the Transformer architecture [31], which is used to compute a sequence representation that associates the element at different positions in a sequence. For input a length- n sequence $X \in \mathbb{R}^{n \times d_m}$ of vectors $x_i \in \mathbb{R}^{d_m}$, the self-attention of X outputs

$$attention(X) = softmax\left(\frac{(XW_q)(XW_k)^T}{\sqrt{d_k}}\right)(XW_v), \quad (15)$$

where $W_q \in \mathbb{R}^{d_m \times d_k}$, $W_k \in \mathbb{R}^{d_m \times d_k}$, and $W_v \in \mathbb{R}^{d_m \times d_v}$ are learnable matrices used to project every $x_i \in X$ from the space of dimension d_m onto a subspace of dimension d_k , d_k and d_v respectively, and $\sqrt{d_k}$ is a scaling factor depending on the subspace dimension. Each row in the output of $attention(X) \in \mathbb{R}^{n \times d_v}$ can be viewed as a new vector representation for the i -th element x_i in the sequence X , which contains the correlated information to another element in a different position.

In our work, we treat the environment full state s as a sequence of length n . For the critic input, the state s_t at every time step is first sent into a linear layer that maps the internal state representation for each agent onto a higher dimensional space. Then, the output from the linear layer, of dimension $\mathbb{R}^{n \times d_m}$, is used to compute the attention output using the matrix equation (15). The final output from attention, denoted as $z_t = attention(s_t)$, is considered as a new representation of environment. In particular, each row of z_t , denoted as z_t^i , is a new representation of s_t^i that contains not only information of the intrinsic state for the i th agent, but also the information

about other agents relevant to coordination in the coverage task. In practice, the attention is often followed by residual connections and layer normalization to facilitate the training, and our implementation preserve this structure as well.

Since the attention output fuses all agents' information while giving each agent different internal state representations, the shared critic network can output different values according to the new representation z^i for different agents. Such structure allows us to use the value decomposition approach (VD) [32], where we explicitly formulate the state value function estimation at time step t as the summation of local state values estimated from every z_t^i , i.e.,

$$V^{\pi_\theta}(s_t) \approx \sum_{i=1}^n V_\phi(z_t^i). \quad (16)$$

We remark that the additive value decomposition is legitimate in our setup due to the explicit additive reward formulation and the true value function, defined as $V^{\pi_\theta}(s_t) = \sum_{i=1}^n \mathbb{E}_{\pi_\theta}[\sum_{k=0}^T \gamma^k R_{t+k}^i | s = s_t]$.

The main advantages of using the VD in our work is to alleviate the credit assignment problem compared to using the global reward R . The direct value decomposition allows us to decompose the advantage function $A_\pi(s, a)$ as well, which accelerates the policy learning further. Moreover, the structure of the shared value network is still a MLP, where the z_t is fed to compute the final local state value for each agent. Note that the new structure of the critic network still agrees with the main feature of the CTDE framework, where a centralized critic network estimates the state value via global information.

E. Training with Behaviour Cloning Regularizer

In order to make the policy training smooth, several techniques and modifications are made to the MAPPO algorithm.

Training is challenging in our task due to sparsity in the reward and nonstationarity in the MARL problem. First, sparse rewards are often problematic in RL problems since they do not provide a useful reward signal for most states. In this work, our reward function (14) is partially sparse since when the agent is outside the domain, the reward is constant; this may cause slow convergence in policy training. Second, nonstationarity is a common challenge in any MARL problem. Since all the agents in the environment are learning simultaneously, the learning process of MARL is often unstable. Both concerns directly relate to the exploration-exploitation trade-off in the RL problem. The sparse reward problem can be alleviated by encouraging exploration among all agents. However, since agents explore to obtain information not only about the environment but also about the other agents, excessive exploration destabilizes the learning dynamics of the other agents, thus making the learning task more difficult.

In this work, we address these two challenges by combining online RL and offline learning with demonstrations. Many previous works have combined online and offline learning in RL problems [33], [34]. Our approach is similar to theirs, but is built on the base of the MAPPO algorithm. The main modification in our approach is adding the BC loss (4) as a regularizer into the MAPPO policy loss given in (2).

With the use of BC, we prepare a set of trajectories D_E obtained from an expert policy f . During training, multiple

trajectories are sampled from the current shared policy π_{θ_k} and stored into a rollout buffer $D_{\mathcal{T}}$ at each iteration. In the update stage, the auxiliary loss L^{BC} is added in the following way. Let G_π denote the expected return of a trajectory generated by policy π :

$$G_\pi = \mathbb{E}_{s_0 \sim \rho_0, a \sim \pi_\theta} \left[\sum_{t=0}^T \gamma^t R(s_t, a_t, s_{t+1}) \right], \quad (17)$$

where ρ_0 is the distribution for the initial state. Hence, G_π is estimated by averaging the returns over all trajectories sampled from the policy π . We further define the performance ratio between the current policy π_{θ_k} and the expert policy f as

$$\xi = \frac{G_{\pi_{\theta_k}}}{G_f} \approx \frac{\frac{1}{|D_{\mathcal{T}}|} \sum_{D_{\mathcal{T}}} \sum_{t=0}^T \gamma^t R_t}{\frac{1}{|D_E|} \sum_{D_E} \sum_{t=0}^T \gamma^t R_t}. \quad (18)$$

By considering the estimated performance ratio ξ , the policy update falls into two cases. When ξ is greater than a positive threshold value, the policy update follows the new loss that combines the CPI objective and BC loss as

$$L^{CPI+BC}(\theta) = -\mathbb{E}_{\pi_{\theta_k}} \left[r_t(\theta) \hat{A}_t^i \right] + \lambda \left(\frac{1}{|D_E|} \sum_{t \in D_E} \|\hat{a}_t^i - \mu_{\pi_\theta}(o_t^i)\|_2^2 \right), \quad (19)$$

where $r_t(\theta)$ is the probability ratio as in (3), \hat{A}_t^i is an advantage estimation for the i th agent, and λ is the adaptive weight given by $\lambda = \frac{e^\xi - 1}{10}$.

For the case of ξ small enough, the policy update will follow the standard clip loss given in (2) on the rollout buffer $D_{\mathcal{T}}$ as

$$L^{Clip}(\theta) = -\mathbb{E}_{\pi_{\theta_k}} \left[\min(r_t(\theta) \hat{A}_t^i, \text{clip}(r_t(\theta), 1 - \epsilon, 1 + \epsilon) \hat{A}_t^i) \right]. \quad (20)$$

Note that both policy losses above assume that action-observation pairs are produced by sampling a shared policy.

Although the policy is trained with D_E when ξ is large enough, the learning of the value function uses only samples in the rollout buffer $D_{\mathcal{T}}$. The value decomposition structure offer two versions of critic loss:

$$L^{Critic}(\phi) = \frac{1}{|D_{\mathcal{T}}|} \sum_{t \in D_{\mathcal{T}}} \left(\hat{V}^i - V_\phi(z_t^i) \right)^2, \quad (21)$$

$$L^{Critic}(\phi) = \frac{1}{|D_{\mathcal{T}}|} \sum_{t \in D_{\mathcal{T}}} \left(\hat{V} - \sum_{i=1}^n V_\phi(z_t^i) \right)^2 \quad (22)$$

For the normal value decomposition structures, (22) is used since the environment only provides the global reward. Here we use (21) since the agents' individual reward can be directly accessed. The value target is chosen to be the Monte-Carlo estimation of agents' individual returns at every time, given by $G_t^i = \sum_{k=0}^T \gamma^k R_{t+k}^i$.

Using the BC loss, our approach allows the policy to be trained toward expert policy at first. When the current policy performs similarly to the expert policy, the drop of the BC loss term allows for a proper exploration to find a better behavior strategy. Here, the exploration-exploitation trade-off is largely controlled by the threshold value for ξ . With an appropriate

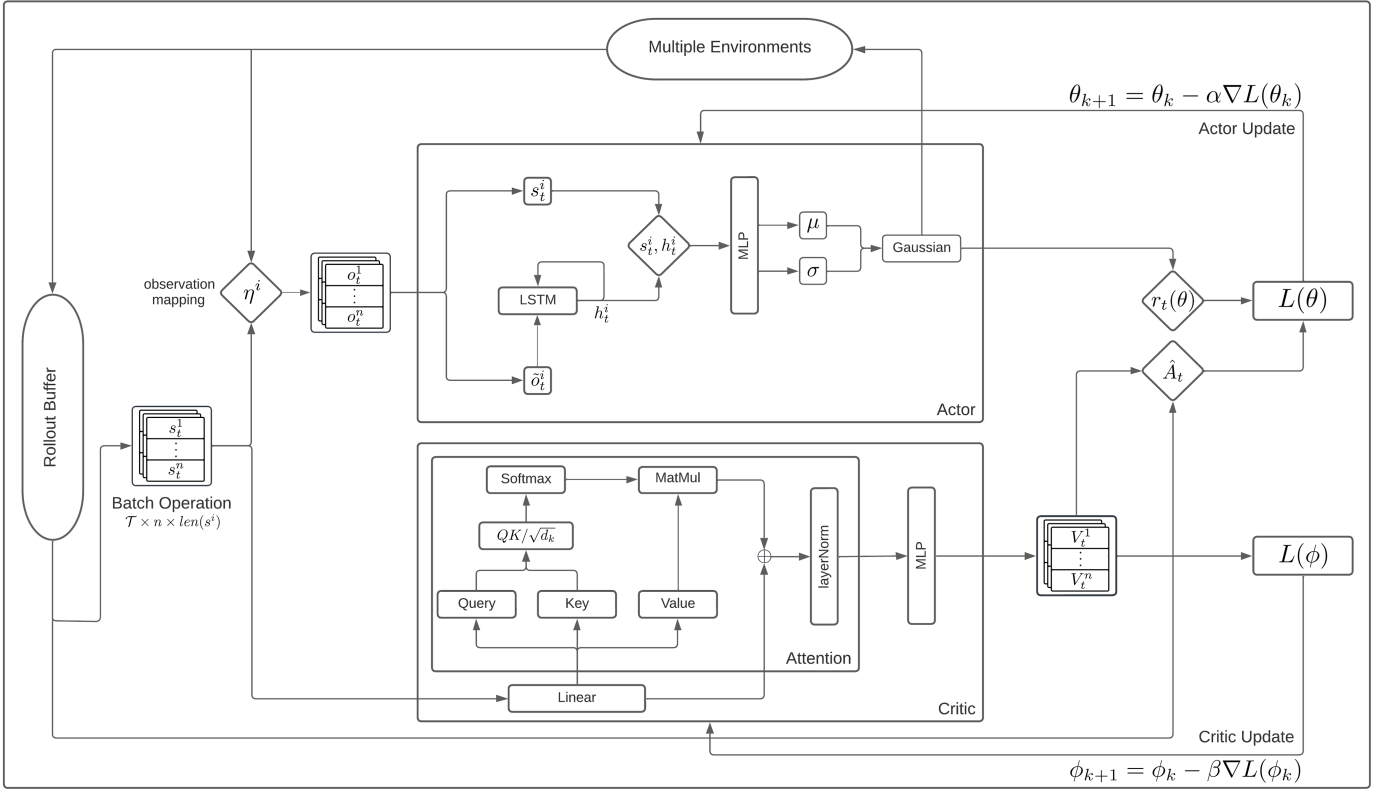


Fig. 2: An overview of our approach.

Algorithm 1: BC regularized PS-MAPPO

Input expert dataset D_E from expert policy f ;
Initialize π_{θ_0} and V_{ϕ_0} ;
for $k = 0, 1, 2, \dots$ **do**
 Sample a set of trajectories from current policy π_{θ_k} and store it into the rollout buffer $D_{\mathcal{T}}$;
 Compute advantage \hat{A}_t^i for every sample in $D_{\mathcal{T}}$ using current value function V_{ϕ_k} ;
 Compute the performance ratio λ_k ;
 if $\lambda_k < \text{threshold}$ **then**
 Update the policy parameter θ_{k+1} using loss given in (20);
 else
 Update the policy parameter θ_{k+1} using loss given in (19);
 end
 Update value function V_{ϕ_k} by the loss given in (21);
end

threshold value, the invalid exploration that results in a policy with lower performance than the expert policy will be cut off.

Moreover, the expert policy chosen in this work is the control law proposed in [11], [22], which can be directly derived from the two potentials U_h and U_I (see (9a) and (9b))

by taking the negative gradient with respect to each agent:

$$a^i = -\nabla_i U_h(p^i) - \sum_{j=1}^n \nabla_i U_I(p^{i,j}) - cv^i, \quad (23)$$

where c is a positive constant. We remark that this controller drives system (1) into an equilibrium configuration which is a critical point of the total system potential energy Φ from (11); note that critical points of Φ are l_d -subcover configurations. For more discussion on the asymptotic behaviour of system (1) with this control law, we refer to [11], [22].

V. SIMULATED EXPERIMENTS

In this section, we present simulation results of the policy obtained by our approach in various domains and across different numbers of agents. We will first compare the performance of a state-of-the-art classical controller and our policy. Then, we show that our approach provides a good model for generalization ability.

In our simulated experiments, the policy is trained in two stages. The first stage is to train a general policy for different numbers of agents by performing parallel sampling on multiple environments involving a different number of agents and different domains. The domain in each environment is a random polygon generated by randomly perturbing the edges of a square with Gaussian noise. After the first stage, a quick fine-tuning is done on the general policy for gaining the best performance in a specific scenario. Fine-tuning on a specific scenario only takes about 100 iterations. The BC loss term is dropped completely during the fine-tuning stage.

All simulations are 30 seconds long. The agents start from an approximately horizontal line configuration outside the domain (with only a slight offset from a perfect horizontal line) and with zero initial velocity.

A. Comparison with State-of-the-Art Classical Controller

We first compare our policy with the state-of-the-art controller (23) on a square domain with 9 agents. For a square domain and a square number of agents, the l_d -subcover configuration is unique and simple, with all agents in a square formation. Fig. 3 shows the agents' positions and trajectories generated by the classical controller (23) (left column) and by our policy (right column). The colored dots represent the agents' positions at the current time, and the dashed tails represent the trajectories for the past 10 seconds.

In the first 10 seconds of the simulation, our policy behaves very differently from the classical controller. For the trajectories generated by the classical controller, an overshooting behavior can be observed. All agents initially enter the domain, but some pass through the domain after entering it. Such overshooting behavior reduces the time efficiency for achieving the final coverage configuration. In contrast, the trajectories from our policy show that all agents directly approach the final l_d -subcover configuration.

For the next 20s, the classical controller brings the overshooting agents back into the domain, then holds all agents within the domain and drives them slowly to the final configuration. Meanwhile, our policy maintains the l_d -subcover configuration with only small perturbations over time.

We also measure the coverage performance using the system potential Φ . Fig. 4 shows the evolution of Φ over time, for the square domain simulation, where the red dashed curve corresponds to the classical controller (23) and the solid blue curve is for our policy. The left plot is for the whole simulation duration, while the right plot gives a zoomed-in view of the last 20 seconds. During approximately the first 5 seconds, the system potential Φ decreases rapidly in both the classical controller (23) and our policy. This behaviour indicates that the overall potential level is much higher when agents are far away from the domain.

The two bumps of the potential energy for the classical controller (at around $t \approx 6$ and $t \approx 10$) can be explained as follows. The first bump occurs when some agents get too close to each other inside the domain, resulting in strong repulsive forces. Such repulsive forces push the agents to get far away from each other so strongly that some agents are pushed out of the domain. This overshoot causes the second bump in Φ – see also Fig. 3 (top left).

In contrast, the solid blue curve shows that for our policy the potential decreases quickly and stays at a low level without any increase. Note that the potential level of our policy is always below that of the classical controller (23), which does not converge to the l_d -subcover configuration within 30s duration.

B. Policy Generalization

We now present simulation results on various domain shapes and across different number of agents. Fig. 5 shows the positions and trajectories of 8 agents that cover a non-convex non-symmetric domain. The plots correspond to the classical

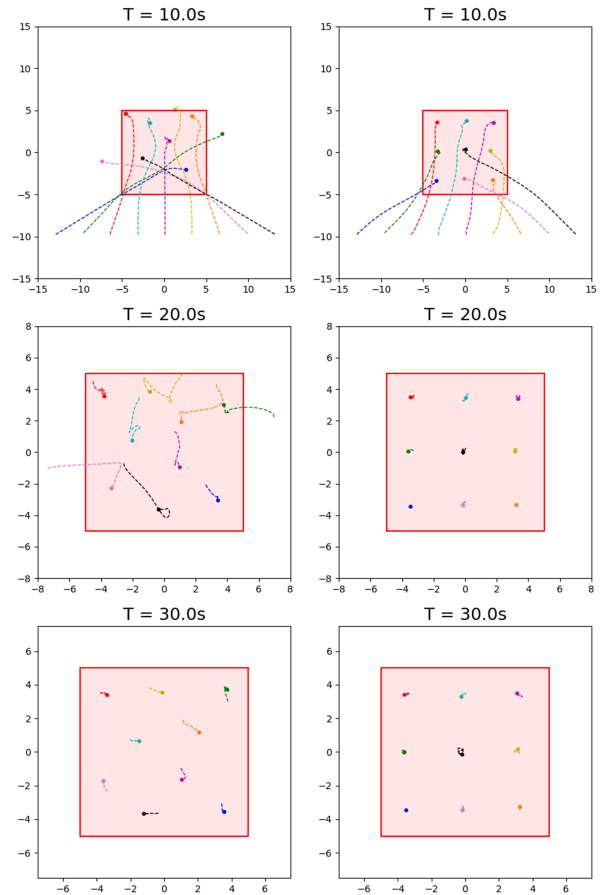


Fig. 3: Square domain coverage of 9 agents for system (1) with classical controller (23) (left) and for our policy (right). All agents start from an approximately horizontal line configuration with zero initial velocity. Note the superior time efficiency of our policy, by which the agents converge to the correct l_d -subcover configuration in only about 10 seconds.

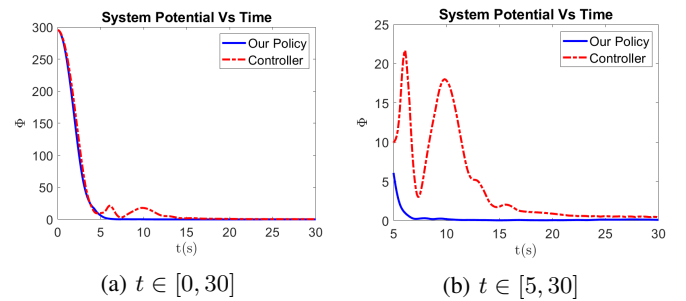


Fig. 4: Time evolution of the total potential energy Φ from (11) for the classical controller (dashed red) and our policy (solid blue). The left plot shows the entire duration and the right plot zooms in on the last 25. The two bumps of the red curve in the left plot are due, respectively, to strong repulsive forces and the overshooting behavior present in the classical controller. The right plot shows that our policy maintains a low potential in the last 20 seconds. Note that the corresponding potential level of our policy is always below that of the classical controller.

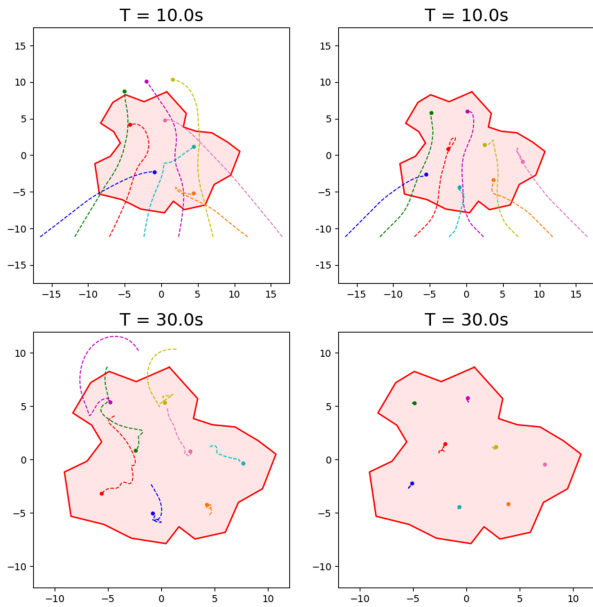


Fig. 5: Non-convex domain coverage of 8 agents for system (1) with classical controller (23) (left) and for our policy (right). All agents start from an approximately horizontal line configuration with zero initial velocity. Our policy has a superior time efficiency for convergence to an l_a -subcover configuration.

controller (left) and to our policy (right). The controller achieves the final coverage configuration within 30 seconds, while our policy only takes about 10 seconds. We note again the overshooting phenomenon present in the controller.

Fig. 1 shows results with 6 to 9 agents, for both symmetric and non-symmetric domains. All four plots in Fig. 1 show the agents' final positions and the trajectories in the last 10 seconds. In all four cases, our policy achieves good coverage within 20 seconds. After reaching the coverage configuration, the agents only exhibit small perturbations, demonstrating the persistent coverage performance of our policy.

REFERENCES

- [1] G. Zhang, G. K. Fricke, and D. P. Garg, "Spill detection and perimeter surveillance via distributed swarming agents," *IEEE/ASME Trans. Mechatronics*, vol. 18, no. 1, pp. 121–129, 2013.
- [2] W. J. Yun, S. Park, J. Kim, M. Shin, S. Jung, D. A. Mohaisen, and J.-H. Kim, "Cooperative multiagent deep reinforcement learning for reliable surveillance via autonomous multi-uav control," *IEEE Trans. Industrial Informatics*, vol. 18, no. 10, pp. 7086–7096, 2022.
- [3] X. Dang, C. Shao, and Z. Hao, "Target detection coverage algorithm based on 3d-voronoi partition for three-dimensional wireless sensor networks," *Mobile Information Systems*, vol. 2019, pp. 1–15, 03 2019.
- [4] W. Wang, V. Srinivasan, K.-C. Chua, and B. Wang, "Energy-efficient coverage for target detection in wireless sensor networks," in *Int. Symposium on Information Processing in Sensor Networks*, 2007.
- [5] D. Drew, "Multi-agent systems for search and rescue applications," *Current Robotics Reports*, vol. 2, June 2021.
- [6] J. P. Queralt, J. Taipalmaa, B. Can Pullinen, V. K. Sarker, T. Nguyen Gia, H. Tenhunen, M. Gabbouj, J. Raitoharju, and T. West-erlund, "Collaborative multi-robot search and rescue: Planning, coordination, perception, and active vision," *IEEE Access*, vol. 8, pp. 191617–191643, 2020.
- [7] J. Cortes, S. Martinez, T. Karatas, and F. Bullo, "Coverage control for mobile sensing networks," *IEEE Trans. Robotics and Automation*, vol. 20, no. 2, pp. 243–255, 2004.
- [8] Y. Cao, W. Yu, W. Ren, and G. Chen, "An overview of recent progress in the study of distributed multi-agent coordination," *IEEE Transactions on Industrial Informatics*, vol. 9, no. 1, pp. 427–438, 2013.
- [9] S. S. Ge and Y. Cui, "Dynamic motion planning for mobile robots using potential field method," *Autonomous Robots*, vol. 13, pp. 207–222, 2002.
- [10] J. Chengcheng, Y. Yajun, and Y. Xuerong, "Distributed area coverage control for multi-agent based on artificial potential field," in *IEEE Int. Conf. Unmanned Systems*, 2019.
- [11] J. Chacon, M. Chen, and R. C. Fetecau, "Safe coverage of compact domains for second order dynamical systems," *IFAC-PapersOnLine*, vol. 53, no. 2, pp. 15167–15173, 2020.
- [12] H. M. La and W. Sheng, "Distributed sensor fusion for scalar field mapping using mobile sensor networks," *IEEE Trans. Cybernetics*, vol. 43, no. 2, pp. 766–778, 2013.
- [13] Y. Tan, "Multi-robot swarm for cooperative scalar field mapping," in *Handbook of Research on Design, Control, and Modeling of Swarm Robotics*, pp. 383–395, IGI Global, 2015.
- [14] M. T. Nguyen, H. M. La, and K. A. Teague, "Collaborative and compressed mobile sensing for data collection in distributed robotic networks," *IEEE Trans. Control of Network Systems*, vol. 5, no. 4, pp. 1729–1740, 2018.
- [15] K. I. Harrington, E. Awa, S. Cussat-Blanc, and J. Pollack, "Robot coverage control by evolved neuromodulation," in *Int. Joint Conf. Neural Networks*, 2013.
- [16] H. X. Pham, H. M. La, D. Feil-Seifer, and A. Nefian, "Cooperative and distributed reinforcement learning of drones for field coverage," 2018. arXiv preprint:1803.07250.
- [17] J. Xiao, G. Wang, Y. Zhang, and L. Cheng, "A distributed multi-agent dynamic area coverage algorithm based on reinforcement learning," *IEEE Access*, vol. 8, pp. 33511–33521, 2020.
- [18] J. Heydari, O. Saha, and V. Ganapathy, "Reinforcement learning-based coverage path planning with implicit cellular decomposition," 2021.
- [19] A. A. Adepegba, S. Miah, and D. Spinello, "Multi-agent area coverage control using reinforcement learning," in *Int. Florida Artificial Intelligence Research Society Conf.*, 2016.
- [20] M. Kouzehgar, M. Meghjani, and R. Bouffanais, "Multi-agent reinforcement learning for dynamic ocean monitoring by a swarm of buoys," in *Global Oceans 2020: Singapore – U.S. Gulf Coast*, 2020.
- [21] R. Lowe, Y. Wu, A. Tamar, J. Harb, P. Abbeel, and I. Mordatch, "Multi-agent actor-critic for mixed cooperative-competitive environments," in *Int. Conf. Neural Information Processing Systems*, December 2017.
- [22] J. Chacon, M. Chen, and R. C. Fetecau, "Safe coverage of moving domains for vehicles with second order dynamics," *IEEE Trans. Autom. Control*, 2022. Early access.
- [23] F. A. Oliehoek and C. Amato, *A Concise Introduction to Decentralized POMDPs*. Springer, 1st ed., 2016.
- [24] C. Yu, A. Velu, E. Vinitzky, Y. Wang, A. Bayen, and Y. Wu, "The surprising effectiveness of PPO in cooperative, multi-agent games," 2022. arXiv preprint: 2103.01955.
- [25] J. Schulman, F. Wolski, P. Dhariwal, A. Radford, and O. Klimov, "Proximal policy optimization algorithms," 2017. arXiv preprint: 1707.06347.
- [26] S. Kakade and J. Langford, "Approximately optimal approximate reinforcement learning," in *Int. Conf. MACHINE LEARNING*, 2002.
- [27] J. Schulman, P. Moritz, S. Levine, M. Jordan, and P. Abbeel, "High-dimensional continuous control using generalized advantage estimation," in *Int. Conf. Learning Representations (ICLR)*, 2016.
- [28] J. K. Gupta, M. Egorov, and M. Kochenderfer, "Cooperative multi-agent control using deep reinforcement learning," in *Autonomous Agents and Multiagent Systems*, 2017.
- [29] J. K. Terry, N. Grammel, S. Son, and B. Black, "Parameter sharing for heterogeneous agents in multi-agent reinforcement learning," 2020. arXiv preprint: 2005.13625.
- [30] S. Hochreiter and J. Schmidhuber, "Long Short-Term Memory," *Neural Computation*, vol. 9, pp. 1735–1780, 11 1997.
- [31] A. Vaswani, N. Shazeer, N. Parmar, J. Uszkoreit, L. Jones, A. N. Gomez, L. Kaiser, and I. Polosukhin, "Attention is all you need," in *Int. Conf. Neural Information Processing Systems*, 2017.
- [32] P. Sunehag, G. Lever, A. Grusl, W. M. Czarnecki, V. Zambaldi, M. Jaderberg, M. Lanctot, N. Sonnerat, J. Z. Leibo, K. Tuyls, and T. Graepel, "Value-decomposition networks for cooperative multi-agent learning based on team reward," in *Int. Conf. Autonomous Agents and MultiAgent Systems*, 2018.
- [33] A. Nair, B. McGrew, M. Andrychowicz, W. Zaremba, and P. Abbeel, "Overcoming exploration in reinforcement learning with demonstrations," in *IEEE Int. Conf. Robotics and Automation*, 2018.
- [34] V. G. Goecks, G. M. Gremillion, V. J. Lawhern, J. Valasek, and N. R. Waytowich, "Integrating behavior cloning and reinforcement learning

for improved performance in dense and sparse reward environments,” in *Int. Conf. Autonomous Agents and MultiAgent Systems*, 2020.